ACS OMEGA

http://pubs.acs.org/journal/acsodf

Article

Enhancement of Uranium Recycling from Tailings Caused by the Microwave Irradiation-Induced Composite Oxidation of the Fe−Mn Binary System

Qingxiang Wang, Tao Huang,* Jing Du,* and Lulu Zhou

Cite This: *ACS Omega* 2022, 7, 24574−24586

Read Online

ACCESS | Metrics & More | Article Recommendations | Supporting Information

ABSTRACT: The extraction of uranium (U)-related minerals from raw ore sands via a leaching procedure would produce enormous amounts of tailings, not only causing radioactivity contamination to surroundings but also wasting the potential U utilization. Effective recycling of U from U tailings is propitious to the current issues in U mining industries. In this study, the influence of the composite oxidation of Fe(III) and Mn(VII) intensified by microwave (MW) irradiation on the acid leaching of U from tailings was comprehensively explored in sequential and coupling systems. The U leaching activities from the tailing specimens were explicitly enhanced by MW irradiation. The composite oxidation caused by Fe(III) and Mn(VII) further facilitated the leaching of U ions from the tailing under MW irradiation in two systems. Maximum leaching efficiencies of 84.61, 80.56, and 92.95% for U ions were achieved in the Fe(III)-, Mn(VII)-, and Fe(III)−Mn(VII)-participated coupling systems, respectively. The inappropriateness of the shrinking core model (SCM) demonstrated by the linear fittings and analysis of variance (ANOVA) for the two systems explained a reverse increase of solid cores in the later stage of leaching experiments. The internal migration of oxidant ions into the particle cores enhanced by MW accelerated the dissolution of Al, Fe, and Mn constituents under acidic conditions, which further strengthened U extraction from tailing specimens.

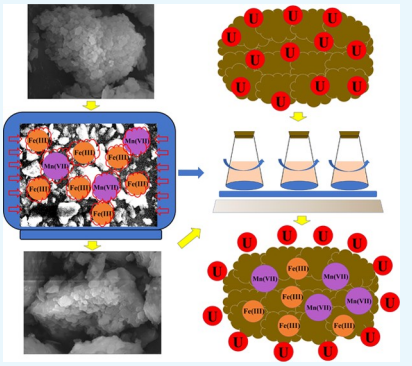

1. INTRODUCTION

The average concentration of U in the crust of Earth is 2−4 ppm (i.e., parts per million), ranking the 51st element in order of abundance. The utilization of uranium has been closely linked to human society since the industrial age, such as to fuel nuclear power plants in the civilian sector and to make high-density penetrators in the military counterpart.[1−3] U is normally extracted from the U-bearing ores by grinding and leaching (e.g., biotic and abiotic) techniques in combination after the mining activities.[4−8] U tailings are produced after U-related minerals and separated from raw ore sands via leaching.[9−11] The U tailings are commonly stored or stacked in huge impoundments, which retains up to 85% of the radioactivity of original U ores emitting to surroundings due to the residual existences of some contained radioactive nuclides such as uranium-238 (^{238}U), uranium-235 (^{235}U), thorium-230 (^{230}Th), and radium-226 (^{226}Ra).[12−14] In China, most of the U tailings are stored in the open air at present. Although the environmental hazards posed by the U tailings have attracted more attention, the old reservoir way is still maintained in some stockpiling regions due to the blurred responsibilities and the shortage of funds.[15−19] Therefore, the radionuclides and some coexisting heavy metals (HMs) contained in the tailings can be potentially migrated into groundwater from the surface by heavy rains and carried great distances by strong winds, finally entering the biological terminals through the food chain and threatening the ecosystem operations.[20−24] The residents can be exposed to uranium and its radioactive daughters by ingesting contaminated food and water and even by inhaling sand dust in the air. Furthermore, long-time uranium exposure will cause severe damage to the normal functioning of some organs (e.g., heart, liver, and kidney) and the nervous system.[25−27]

Until now, the treatment technologies mentioned for the U tailings include physical segregation (e.g., backfilling and soil covering), biohydrometallurgy, phytoremediation, solidification/stabilization (S/S), chemical leaching, etc.[28−33] Specifically, the physical segregation method can effectively reduce the land area occupied by U tailings and obstruct the radiative emittance into the air within a short period. However, the segregation technique makes the accumulation and further infiltration of radionuclides easier during long-term weathering processes.[28,34] The recent progress in biohydrometallurgy for mining has been reported in several reviews.[35] More other enhancements are necessarily put forward for the microbe-

Received: April 17, 2022
Accepted: June 29, 2022
Published: July 6, 2022

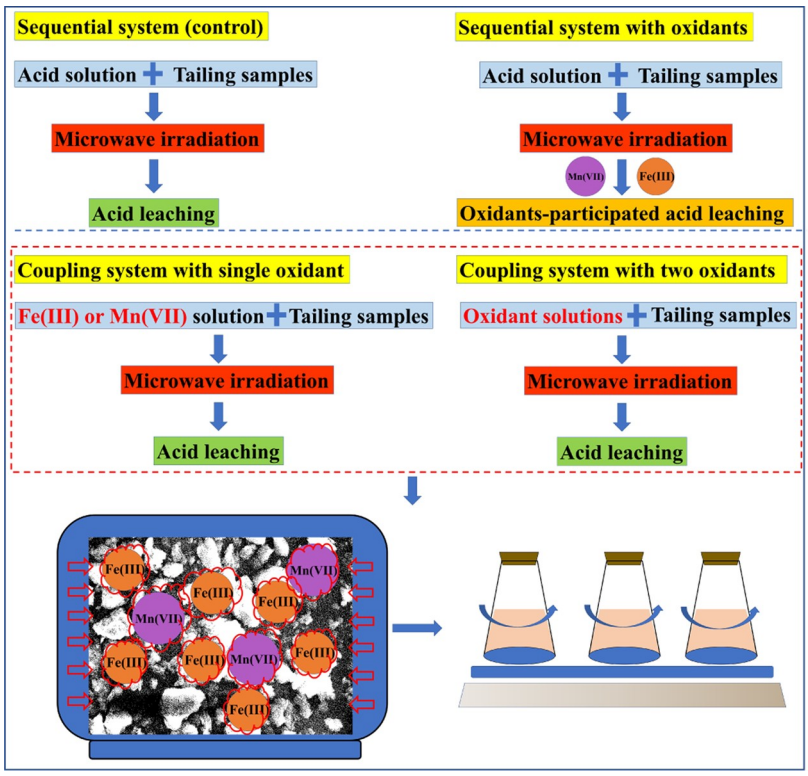

Figure 1. Flow diagram of the microwave irradiation-participated leaching process for treating uranium tailing samples.

related activities to overcome the inapplicability of biohydrometallurgy to the refractory U tailings.[35,36] The phytoremediation method utilizes some plants to effectively adsorb radionuclides from contaminated aquifers or soils, reducing the migration and diffusion of radionuclides on the surfaces.[37−40] However, the contaminated plants need real-time monitoring and timing harvesting and postdisposal. Some radionuclides can be rashly brought into the biosphere through the intermediary role of some plants. The solidification/stabilization (S/S) can immobilize the relevant radionuclides and correspondingly lower the bioavailability in a relatively safe way, while its application is severely limited by the insufficient cost and storage spaces.[41−45] Moreover, the S/S reduces the possibility of the secondary recycling of U tailings and the recovery of some radionuclides. Therefore, it is necessary to explore a more reliable method to extract U from U tailings, which is not only beneficial to the resource utilization of tailings but also conducive to achieving better treatment performances using the current technologies.

Commonly, the low content percent of carbonate minerals means that the acid lixiviants combined with some surfactants and oxidants are used to treat the U tailings in preference.[12,14,46] However, the refractory characteristics of U tailings caused by the gangue compositions and the residuals in all links will consume much higher acid concentrations or more complexing agents, trying to elevate the efficiency levels during the leaching process.[11,17,47−50] Correspondingly, the costs will be surprisingly increased, and more engineering legacy issues such as secondary pollution and ecological remediation will be produced. Some appropriate pretreatments and enhancements should be explored to avoid the dependence on higher acid concentrations. The microwave (MW) irradiation technique has been widely applied in intensifying the chemical activities of materials.[51−53] MW can change the mineral microstructures and accelerate the dispersion of chemical reagents in the pores and fissures by intensely activating the vibrations of polar molecules in a very short time.[54] MW irradiation has achieved remarkable results for the fabrication and synthesis of different functionalized materials.[55,56] However, the comprehensive employment of MW in mining engineering has been rarely studied, especially for the hydrometallurgical engineering of refractory mineral ores.

In this study, the MW irradiation coupling with the oxidants of Fe(III) and Mn(VII) was exploratorily employed in the conventional sulfuric leaching process in two different forms to enhance the acid leaching of U ions from the low-degraded tailing samples. The influence of MW irradiation and the relevant mechanisms have been comprehensively investigated. Generally, there are several main aims of this study: (i) to study the effects of hydrometallurgical parameters on the leaching efficiencies of U in a sequential system, (ii) to optimize the coupling system and quantitively analyze the significances of variables, (iii) to simulate kinetic modeling for two leaching systems, and (iv) to explore the reaction mechanisms and discuss on the leaching behaviors in MW irradiation. The study will supply data support for the broader application of MW in mining and recycling and propose an alternative to the treatments of environmental issues caused by U tailings.

2. METHODS AND MATERIALS

2.1. Chemicals and Sampling Materials. Three kinds of strong acid solutions, including nitric acid (HNO_3, ACS, 70%), hydrofluoric acid (HF, AR, ≥40%), and perchloric acid ($HClO_4$, AR, 70.0−72.0%), were purchased from Aladdin Industrial Corporation and used to prepare the digestion solution for the microwave digestion process. Sulfuric acid (H_2SO_4, 98%) and sodium hydroxide pellets (NaOH, AR)

https://doi.org/10.1021/acsomega.2c02392
ACS Omega 2022, 7, 24574−24586

Table 1. Orthogonal Design with the Experimental Results (Analyzed using ANOVA)[a]

						leaching efficiencies of U ions (%)		
no.	A[b]	B[c]	C[d]	D[e]	E[f]	Fe(III)	Mn(VII)	Fe + Mn
1	2 (4)	2 (0.5)	5 (0.3)	1 (10)	2 (25)	52.94	47.62	58.23
2	5 (10)	5 (2.0)	2 (0.15)	1	5 (40)	81.07	78.96	90.44
3	3 (6)	4 (1.5)	5	2 (30)	1 (20)	66.42	63.95	79.92
4	5	2	4 (0.25)	3 (60)	1	78.34	76.23	88.26
5	1 (2)	5	5	5 (120)	3 (30)	65.18	62.67	81.63
6	5	3 (1.0)	5	4 (90)	4 (35)	74.93	72.55	85.73
7	2	1 (0.1)	4	5	4	60.59	56.63	73.82
8	3	2	3 (0.2)	5	5	57.46	52.48	68.55
9	3	1	2	4	2	54.49	49.83	62.48
10	1	1	1 (0.1)	1	1	42.68	38.75	49.73
11	4 (8)	1	5	3	5	56.74	43.56	66.39
12	4	2	1	4	3	76.82	74.29	87.69
13	2	5	3	4	1	71.36	67.35	82.46
14	1	4	4	4	5	64.15	60.37	78.14
15	5	1	3	2	3	58.83	54.69	70.46
16	3	3	4	1	3	75.39	73.58	86.24
17	4	4	3	1	4	82.36	78.94	90.89
18	1	3	3	3	2	63.72	59.27	76.83
19	3	5	1	3	4	72.57	71.42	84.52
20	1	2	2	2	4	62.35	57.59	75.49
21	2	4	2	3	3	80.39	78.23	89.36
22	4	3	2	5	1	83.46	79.34	91.54
23	2	3	1	2	5	70.52	65.88	82.97
24	5	4	1	5	2	84.61	80.56	92.95
25	4	5	4	2	2	79.72	77.48	88.94

[a]Experimental conditions: the ratio of solid to liquid of 0.1 mg/L, the leaching time of 120 min, the temperature of 30 °C, and the oxidant ratio of Fe(III) to Mn(VII) of 3. [b]Microwave time (min). [c]H_2SO_4 concentrations (M). [d]Oxidant concentrations (M). [e]Leaching time (min). [f]Leaching temperatures (°C).

obtained from SINOPHARM were used to adjust pH in solutions during the experiments. Uranium (V, VI) oxide (U_3O_8, AR) applying for the preparation of uranium standard solution was procured from DINGTIAN Chemical Co., Ltd., Xi'an, China. The oxidants including ferric sulfate ($Fe_2(SO_4)_3$, AR) and potassium permanganate ($KMnO_4$, GR) were purchased from GAIQI Reagent Factory, Jiangsu, China. Deionized (DI) water was used to prepare solutions and conduct experiments. All of the glass containers and gadgets were rinsed three times with DI water and dried before experiments. The tailing samples used in this study were sampled from a uranium tailing-stacking area in Hunan Province, China, stocked, and managed according to two national standards (i.e., EJ/T983 and EJ/T1121). The samples were thermally dried at 105 °C for 12 h, mechanically milled at 160 rpm over 2 h, sifted through a sieve (pore diameter: 75 μm), and packed in waterproof nylon cloths for the further leaching experiments.

2.2. Leaching Procedures and Experimental Designs.

For the conventional acid leaching procedure, the tailing samples were added to H_2SO_4 solutions (200 mL) at a ratio of solid to liquid of 0.1 (g/mL). H_2SO_4 concentrations were adjusted ranging from 0 to 1.5 M. The mixtures were magnetically stirred at 160 rpm and temperatures of 20−40 °C over 120 min. Two milliliters of the mixture was taken out from the reactor using a syringe (10 mL) every 20 min and centrifuged at 8000 rpm over 5 min by a centrifuge. The supernatants separated from the mixtures were used to monitor the changes in the leaching concentrations of uranium during the whole experimental process. Fe(III) and Mn(VII) solutions (0.01−0.3 M) were prepared by dissolving some certain masses of $Fe_3(SO_4)_2$ and $KMnO_4$ using 1.0 M H_2SO_4 solutions, respectively. The oxidant solutions consisting of Fe(III) and Mn(VII) solutions (i.e., Fe + Mn) were used for microwave irradiation-enhanced experiments. In terms of leaching experiments with oxidants, the tailing samples were added to oxidant solutions with the experimental conditions being maintained as the conventional leaching process. The participation of microwave irradiation in the oxidant-assisted leaching process is shown in Figure 1. The microwave-participated treatments were carried out in a microwave reactor (MULTIWAVE PRO, Anton Paar GmbH, Austria). The microwave irradiation experiments were categorized into two different systems by the module combination: (i) the sequential system including microwave pretreatment and sequential oxidant-participated leaching experiments and (ii) the coupling system of the microwave irradiation combined with the leaching experiments with oxidants. Specifications of the sequential system are listed in detail in Table S1 in the supporting information (SI). The experiments for the coupling system were arranged by an orthogonal design with five variables and five levels. The variables are correspondingly illustrated in Table S2 in the SI. The orthogonal design with the experimental results (i.e., leaching efficiencies) is shown in Table 1. The shrinking core model (SCM) was used to analyze the mechanism of U release for both sequential and coupling systems and describe the specific reaction pathways for the kinetic leaching process. The corresponding formula or equations and parameters are specified in the SI (eqs S1−S3).

https://doi.org/10.1021/acsomega.2c02392
ACS Omega 2022, 7, 24574−24586

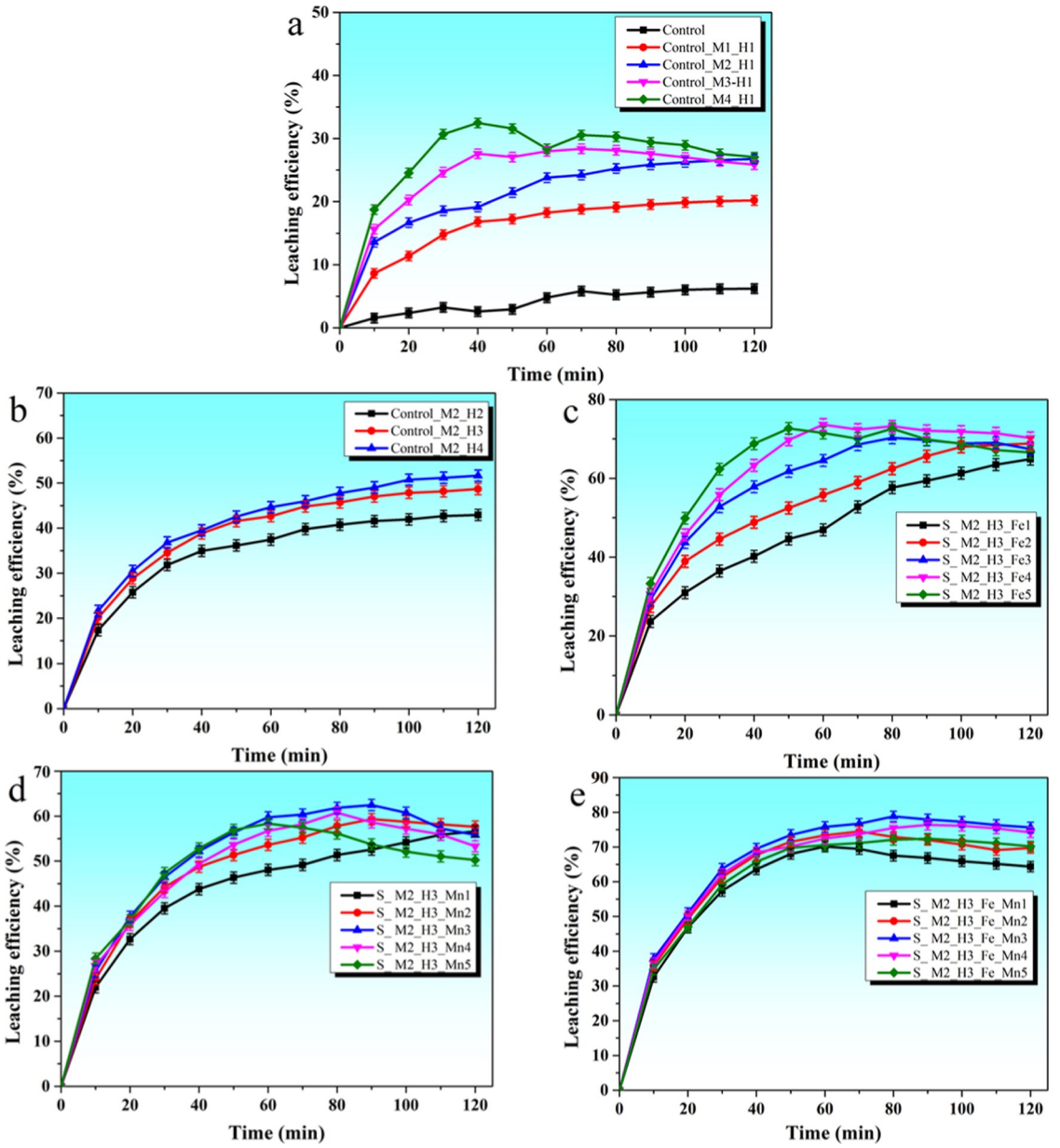

Figure 2. Leaching efficiencies affected by the changes in hydrometallurgical parameters, including the microwave times (a), H_2SO_4 concentration (b), the oxidant concentrations of Fe(III) (c), the oxidant concentrations of Mn(VII) (d), and the oxidant ratios of Fe(III) to Mn(VII) (e) in the sequential system.

2.3. Calculations and Analytical Methods. The tailing samples were chemically digested at a temperature of 30 °C following a Chinese National Standard (EJ/T550-2000). The total concentration (mg/L) of U in the digestion solution and the leaching concentration (mg/L) of U in the leachate were determined using inductively coupled plasma optical emission spectroscopy (ICP-OES, Agilent 7500). The detection process was conducted in triplicate with the standard deviations being maintained at less than 5%. The leaching efficiency (r_t, %) of U from the tailing samples was calculated by eq 1

$$r_t = \frac{c_t \times V_l}{c_c \times V_c} \times 100\% \quad (1)$$

where c_t and c_c are the leaching concentration (mg/L) of U in the leachate at time t and the total concentration (mg/L) of U in the digestion solution, respectively, V_l and V_c represent the corresponding volumes (L) of leachate and digestion solution, respectively. The significance of variables on the leaching in the orthogonal design was analyzed using the analysis of variance (ANOVA). The significance probabilities (Sig.) were calculated by the type III sum of squares, mean squares, and F values in a sequence. The marginal means affected by each variable were evaluated using Tukey's test ($p < 0.05$, default $\alpha = 0.05$).

2.4. Characterization Strategies and Methods. The elemental composition of the raw uranium tailing samples was measured using an X-ray fluorescence spectrometer (XRF, MXF-2400, SHIMADZU, Japan). The results are correspondingly listed in Table S3 in the SI. The chemical speciation of U in the tailing specimens was determined by a modified BCR method,[42] fractionating into four partitions, including acid extractable (P1), reducible (P2), oxidizable (P3), and residual

https://doi.org/10.1021/acsomega.2c02392
ACS Omega 2022, 7, 24574−24586

(P4). The morphologies of specimens before and after the leaching experiments were assessed by a scanning electron microscope (SEM, Carl Zeiss AG, Germany). Meanwhile, the elemental compositions in the selected area of specimens were determined by an energy-dispersive spectrometer (EDS, Carl Zeiss AG, Germany). The changes in minerals were analyzed by an X-ray diffractometer (XRD-6000, SHIMADZU, Japan) with Cu Kα radiation over 2θ ranging from 5 to 80°. The minerals were identified and matched by MDI Jade 6.0 equipped with the JCPDS PDF-2 database. The FTIR spectra and TGA curves were obtained by a Fourier transform infrared spectrometer (Thermo Electron Co., 380 FTIR) over the wavenumber range of 400−4000 cm^{-1} at every step of 4 cm^{-1} and a TGA analyzer (STA 449F3, NETZSCH, Germany) over the temperature range of 25−1500 °C at a heating rate of 10 °C/min, respectively, to assist with the analysis on the changes in the minerals and elements before and after the leaching experiments.

3. RESULTS AND DISCUSSION

3.1. Effects of Hydrometallurgical Parameters in a Sequential System. The leaching efficiencies of U of the tailing samples influenced by the changes in hydrometallurgical parameters in the acid leaching experiments are shown in Figure 2. A control run was set with the specimens only being stirred in DI water over time and used to eliminate the influence of dissolvable uranyl ions adsorbed on the tailing particles from the evaluations of WM irradiation, acid dissolution, and oxidant participation on the sequential running performances. The operating time for MW irradiation treating the specimens before the leaching procedures was adjusted ranging from 3 to 12 min. It was clear that the MW treatment enhanced the leaching activities of specimens for U species and correspondingly brought higher leaching efficiencies compared with that of the control counterpart. MW irradiation with 3 and 6 min was beneficial to the cumulative increases in the leaching efficiencies of specimens over the whole leaching process. However, a longer MW time such as 9 and 12 min would gradually reduce the extraction efficiencies of U using 0.1 M of sulfuric solution in the middle and later stages of leaching experiments (Figure 2a), which was attributed to the imbalance between the MW caused fissure expansion and the microstructural collapse in the tailing specimen.[57] Differently, after 6 min of WM treatment, the increases in H_2SO_4 concentrations (M) steadily elevated the extraction of U from tailing samples (Figure 2b). The participation of the Fe(III) oxidant explicitly further strengthened the acid leaching (1.0 M) for the U tailings after WM irradiation. The addition of 0.1−0.2 M Fe(III) to the solutions facilitated the dissolution acceleration of U species from some minerals in the tailing particles, achieving steady increases in the leaching efficiencies over time. However, too many Fe(III) ions (e.g., 0.25 and 3 M) existing in the acid solutions would play a negative role in promoting U dissolution. The decreasing leaching trends shown in the later phase of experiments directly reflected the readsorption of dissolved U ions (Figure 2c), which was possibly associated with the electrostatic adsorption caused by the formation of some iron species.[58,59] Similar to Fe(III) oxidants, Mn(VII) attended leaching processes and obtained higher extraction results in contrast to that of pure acid experiments. It was noteworthy that Mn(VII) showed stronger adsorption characteristics compared to Fe(III) species with a typical inverted U-shaped leaching curve being obtained at the concentration of 3.0 M (Figure 2d). The coexistence of the two kinds of oxidants in the acid leaching solutions performed more excellent features in boosting the extraction of U from the solid samples (Figure 2e). The oxidant ratio of Fe(III) to Mn(VII) of 3 was most conducive to getting the high leaching efficiencies of U among the four ratio choices. The joint use of Fe(III) and Mn(VII) at specific ratios after the MW irradiation not only enhanced the leaching performances of the sequential system but also relieved the reabsorption drawback to some extent.

3.2. Significance of Variables and Orthogonal Optimization in the Coupling System. The tests of intersubjective effects based on the leaching efficiencies of U obtained in the orthogonal design in the coupling systems (default α: 0.05) are shown in Table S4 in the SI. The marginal means of variables calculated by the sum of squares (type III) are correspondingly displayed in Figure S1 in the SI. The R-squares (i.e., R^2) for the three sources including Fe(III), Mn(VII), and Fe(III) + Mn(VII) were 0.978, 0.997, and 0.956, respectively, with all three adjusted R^2 (i.e., Adj. R^2) being higher than 0.7, indicating that the significance analysis was reliable for the optimal determination. Considering the Fe(III) source, the significance probabilities (i.e., Sig.) of variables were 0.012, 0.005, 0.096, 0.610, and 0.345, respectively, which indicated that both the microwave time (min) and H_2SO_4 concentrations (M) had a significant effect on the leaching efficiencies of U ions in the coupling system. The significance order for the parametrical variables in the orthogonal design descended as H_2SO_4 concentrations (B, M) > microwave time (A, min) > oxidant concentrations (C, M) > leaching temperatures (E, °C) > leaching time (D, min). In terms of the Mn(VII) source, the Sig. values of three variables including A (min), B (M), and C (M) were all lesser than the default α, meaning the changes in the mentioned three variables significantly influenced the U extraction from the tailing particles after the coupled treatments by the oxidant Mn(VII) and MW irradiation. The influence order for variables was sorted as the same as that of source Fe(III). Similarly, for the source of Fe(III) + Mn(VII), the significance order was still maintained with only the variable of B (M) impressively dominating the leaching process in the coupling system and the variable of A (min) having an impact on the whole process. The synergy between the oxidants and MW had been intensified in the coupling system according to the analysis results in the orthogonal experiments. The sulfuric concentrations among the five variables played a prerequisite role in influencing the significance of the other four variables in the whole process. As shown in Figure S1 in the SI, for the source Fe(III), the maximum r_t values were attained at the microwave time (min) of 8 (A_4), H_2SO_4 concentrations (M) of 1.5 (B_4), oxidant concentrations (M) of (C_2), leaching time (min) of 60 (D_3), and leaching temperature of 30 °C (E_3). Correspondingly, for the sources of Mn(VII) and Fe(III) + Mn(VII), the maximum r_t values were obtained at the parametrical combination of $A_5B_4C_2D_5E_3$ and $A_5B_4C_4D_5E_3$, respectively. The marginal mean obtained at the fourth level of A (min) was close to the fifth counterpart referring to all three sources. Similar situations were pinpointed in the third and fifth levels of D (min). Therefore, the optimal combination of variables for the coupling system was finally determined as $A_4B_4C_2D_3E_3$. Generally, unlike the sequential system, A (min) and B (M)

https://doi.org/10.1021/acsomega.2c02392
ACS Omega 2022, 7, 24574−24586

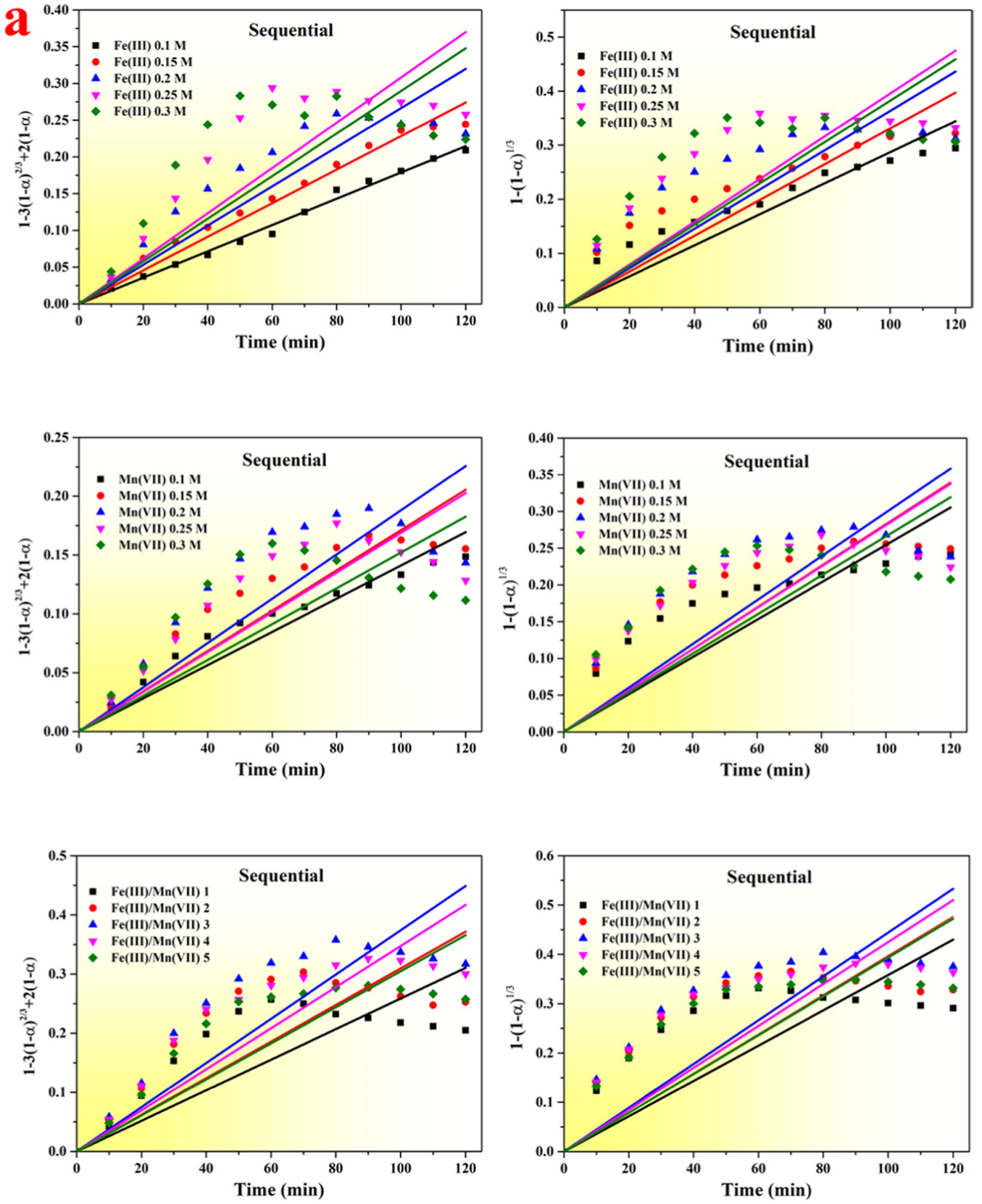

Figure 3. continued

https://doi.org/10.1021/acsomega.2c02392
ACS Omega 2022, 7, 24574−24586

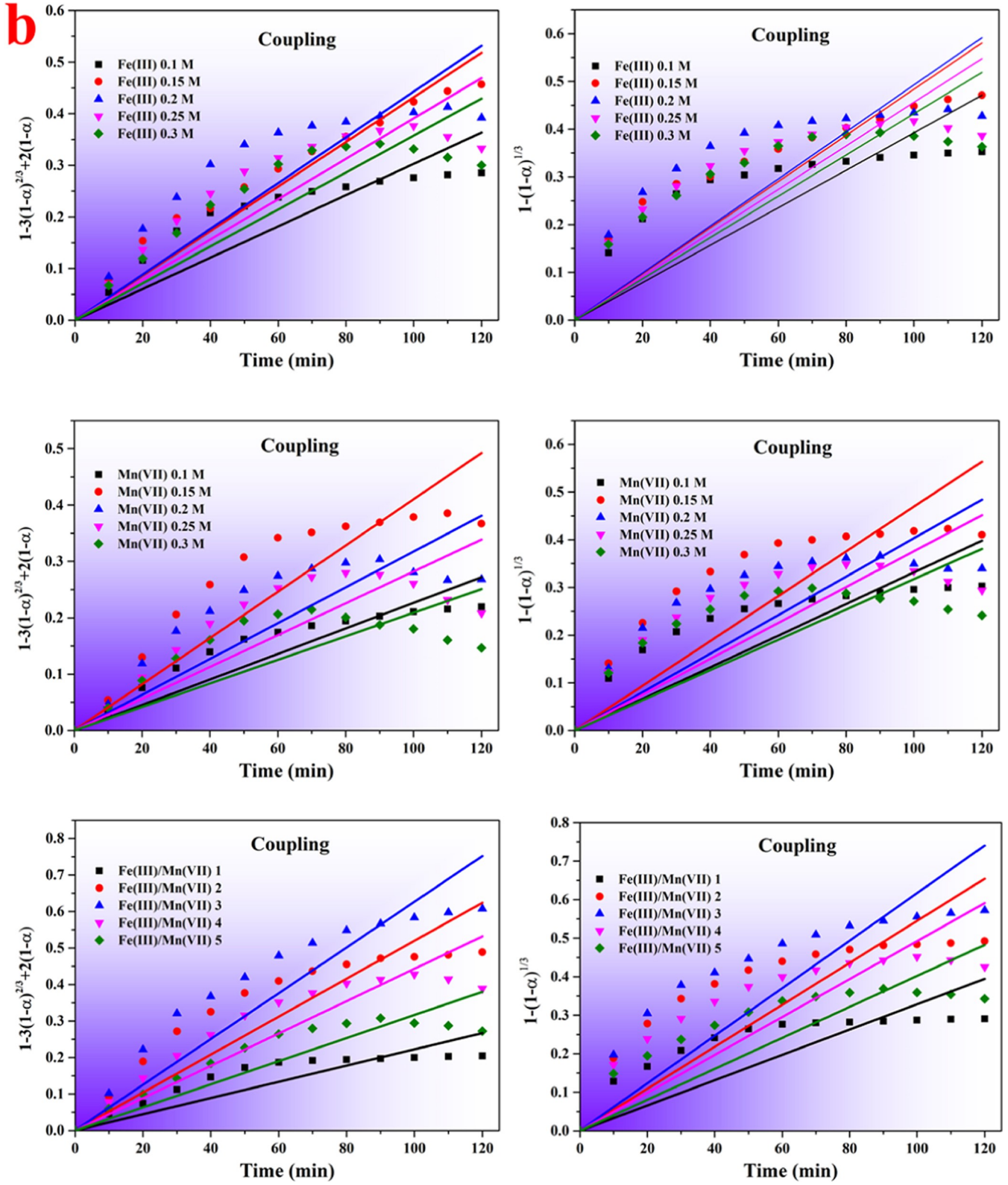

Figure 3. SCM fittings affected by the participation of oxidants in the sequential (a) and coupling (b) systems.

showed a more remarkable impact on the operation of the coupling system compared with the other three variables.

3.3. Kinetic Modeling for Two Leaching Systems. The SCM fittings affected by the participation of oxidants in sequential and coupling systems are shown in Figure 3. The parametrial results of SCM obtained from the fitting analysis are correspondingly listed in Table S5 in the SI. As known, the desired minerals are dissolved in the liquid phase while undesired constituents remained during the leaching process, which further causes varying degrees of shrinkage to the diameter of the unleached core.[60−62] The SCM model is commonly used to mathematically describe this process. As

https://doi.org/10.1021/acsomega.2c02392
ACS Omega 2022, 7, 24574−24586

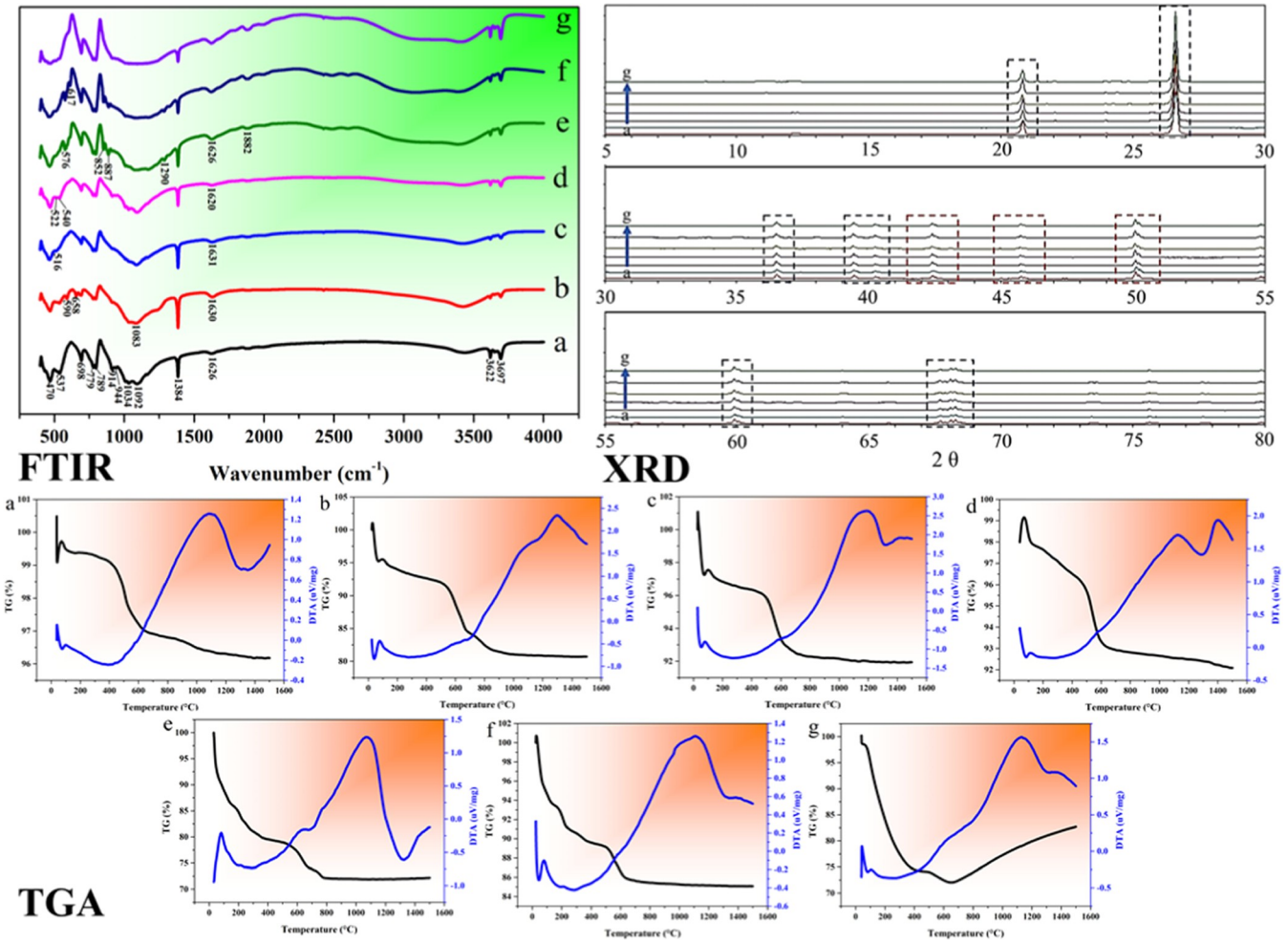

Figure 4. Changes in mineral compositions characterized by FTIR spectra, TGA curves, and XRD: (a) Raw uranium tailing sample, (b) mixture of tailing specimen and Fe(III)−Mn(VII) oxidants, (c) mixture of the tailing specimen and Fe(III)−Mn(VII) oxidants after microwave irradiation, (d) specimen obtained from the leaching experiments, (e) specimen obtained from the Fe(III)−Mn(VII)-participated leaching experiments, (f) specimen obtained from the sequential system, and (g) specimen obtained from the coupling system.

seen, in terms of the whole leaching period (i.e., 120 min), the SCM model including two reaction cases (SI) was generally inappropriate for quantitively illustrating the leaching processes for sequential and coupling systems with the participation of different oxidants and oxidant concentrations.[63,64] The Adj. R^2 values in the parametrical results (Table S5, SI) chimed with the fitting curves for the most part. Notably, the fittings were excellent at the Fe(III) concentration of 0.1 M, which indicated that the low concentration of the oxidant Fe(III) hardly influenced the acid leaching pathways of U tailings and by which the applicability of the SCM model was still acceptable. The whole leaching process was dynamically controlled by the pore diffusion (eq S1, SI) and the heterogeneous surface reactions (eq S2, SI) at the early stage of experiments, rather than the pore diffusion or the heterogeneous reactions at a certain time. However, the appropriateness of the SCM model sharply deteriorated in the middle and late stages of the leaching experiments (i.e., particularly after 60 min) with the increase of Fe(III) concentrations and the participation of Mn(VII). The unleached solid cores in the U tailing particles had endured a reverse increase after the first shrink process over time, which may be subjected to the re-desorption and surface covering caused by the formation of some new Fe−Mn species during the experiments.[65,66]

3.4. Explorations of Reaction Mechanisms.

3.4.1. Changes in Mineral Compositions. The changes in the mineral compositions of U tailing specimens before and after different leaching experiments characterized by FTIR, TGA, and XRD are shown in Figure 4. The peaks at wavenumbers of about 470, 537, 698, 779, 789, 914, 944, 1034, 1092, 1304, 1626, 3622, and 3697 cm^{-1} were observed in the spectrum curve of the raw U tailing sample. The peak at 779 cm^{-1} was directly attributed to the existence of $(UO_2)^{2+}$ stretching vibration in the mineral constitution,[29,67,68] which was further proved by the XRD pattern of the raw uranium tailing sample (Figure S2, SI). The bands at 470, 1304, 1626, 3622, and 3697 cm^{-1} had barely changed after different leaching experiments, which were directly assigned to the gangue or inert constituents contained in the mineral, such as Si−O−Si bending vibration and Si−O and P−O symmetric and asymmetric stretching.[69−71] The band at 1083 cm^{-1} in the spectrum of the mixture specimen was ascribed to SO_2 asymmetric and symmetric stretching, which verified the addition of ferric sulfate to the tailing particles.[72−74] After MW irradiation, the raw band at 537 cm^{-1} was shifted left to the band at 516 cm^{-1}, which reflected the transformation of

https://doi.org/10.1021/acsomega.2c02392
ACS Omega 2022, 7, 24574−24586

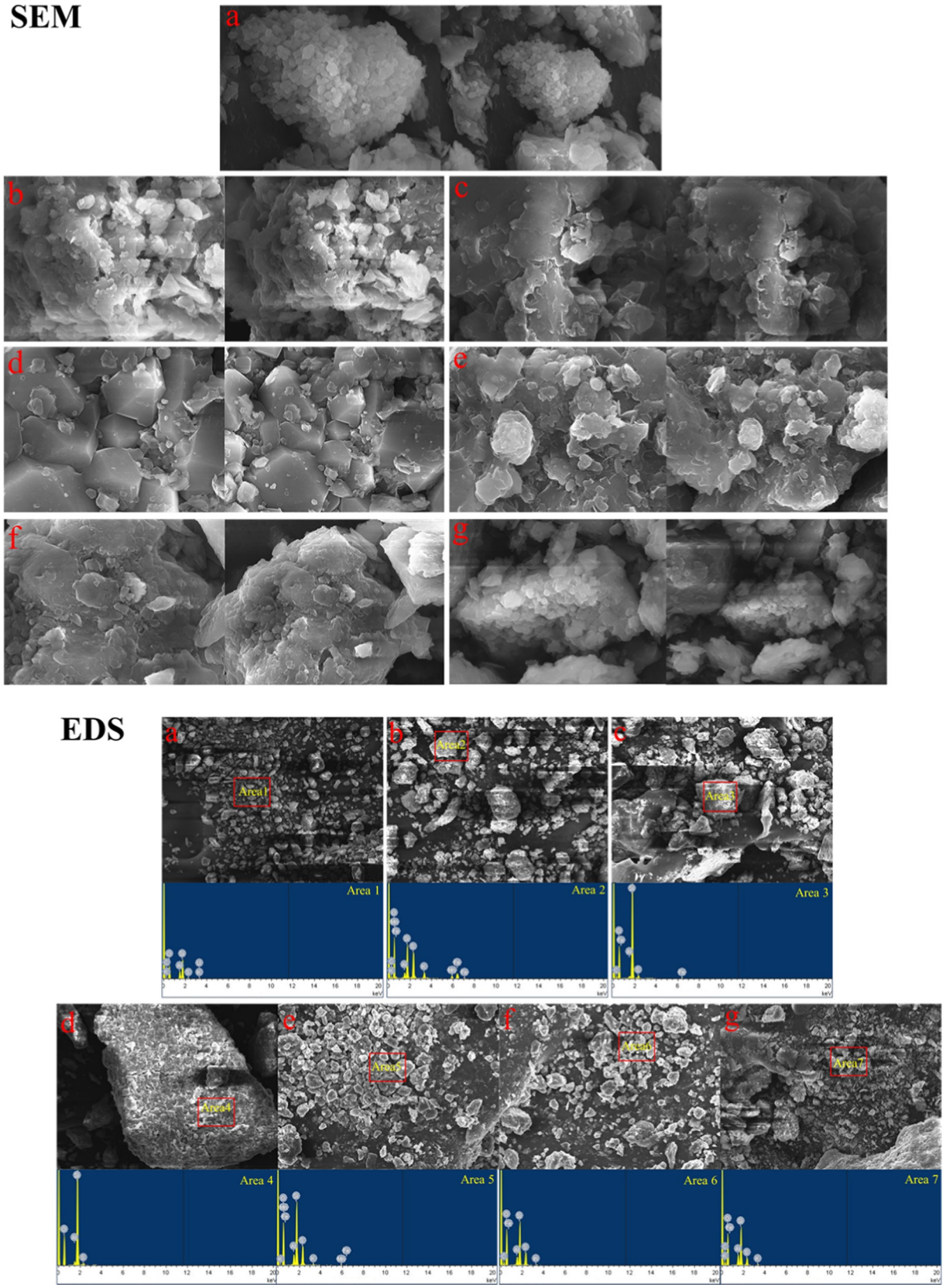

Figure 5. Morphological and elemental changes characterized by SEM and EDS: (a) raw uranium tailing sample, (b) mixture of the tailing specimen and Fe(III)−Mn(VII) oxidants, (c) mixture of the tailing specimen and Fe(III)−Mn(VII) oxidants after microwave irradiation, (d) specimen obtained from the leaching experiments, (e) specimen obtained from the Fe(III)−Mn(VII)-participated leaching experiments, (f) specimen obtained from the sequential system, and (g) specimen obtained from the coupling system.

https://doi.org/10.1021/acsomega.2c02392
ACS Omega 2022, 7, 24574−24586

crystalline silicate to the partial amorphous phase.[70−72] The emergence of the peak at 516 cm^{-1} for the specimen obtained from the sulfuric leaching revealed the substitution of Al^{3+} in the octahedral lattice by H^+ ions. The result demonstrated the dissolution of some minerals from the specimen by the sulfuric solution. Some bands at 576, 617, 887, and 1290 cm^{-1} were formed after the sequential experiments, which explained the participation of oxidants and the generation of derived Fe and Mn species.[65,75,76] Fewer peaks were found in the spectrum of specimens acquired from the coupling experiments. The MW combined with oxidant participation was more conducive to strengthening the effect of acid leaching on the U extraction from the U tailing specimens. The widths of peaks distributed in the 2θ range of 41−52° in the XRD patterns gradually narrowed from specimen a to specimen g (XRD a−g, Figure 4), which echoed with the FTIR results, indicating that the employment of Fe(III)−Mn(VII) oxidants and MW irradiation facilitated the U extraction from the tailing in the acid leaching conditions, and the coupling system was preferable in obtaining higher U leaching results compared with the sequential counterpart (Figure 2). Mass losses of around 4, 20, 8, 8, 30, 16, and 20% were achieved after the thermal decomposition over 1500 °C for specimens of a−f, respectively (TGA a−g, Figure 4). Moreover, the changes in the exothermic and endothermic peaks reflected the relative contents of thermally active constitutions in the specimens. After 700 °C, the mass rebound accompanied by an obvious exothermic peak explicitly verified the formations of some new constituents in the specimens obtained from the coupling system (TGA g, Figure 4), which explained the potentially oxidant-participated chemical reactions in the MW atmosphere and the activation of more unleached constituents in the U tailing particles in the coupling system.

3.4.2. Morphological Characterization. Morphological and elemental changes characterized by SEM and EDS for the different specimens are shown in Figure 5. The elemental compositions (wt %) of different tailing specimens are correspondingly listed in Table S6 in the SI. Granular- and sulcus-like morphologies were observed for the raw U tailing particles, which visually reflected the gangue wrapping to the as-leached mineral constituents (SEM a, Figure 5). Some small cracks and clefts were formed in the mixture of tailing specimens and Fe(III)−Mn(VII) oxidants (SEM b, Figure 5). The participation of oxidants preliminarily activated the tailing specimen. After the MW activation, more macropores were formed in the tailing particles with the participation of oxidants (SEM c, Figure 5), indicating the enhancement to the mineral activation brought by MW. Some regular polyhedrons were seen in the specimen obtained from the leaching experiments (SEM d, Figure 5), which further supported the existence of the unleached gangue constituents in the raw U tailings and also verified the analysis accuracy of mineral compositions (Figure 4). Differently, tubercular and lamellar morphologies were determined after the oxidant-participated leaching experiments (SEM e and f, Figure 5). The Fe(III)−Mn(VII) oxidants had experienced dissolution and regeneration in the acid leaching environment. Larger rifts and contrarily smaller particles were observed in the specimen obtained from the coupling system (SEM g, Figure 5), directly demonstrating the dissolution of more mineral constituents and proving the rationality of kinetic analysis mentioned in the SCM fittings (Figure 3). The elements containing O, Al, Si, S, K, Fe, and U, etc., were matched in EDS, which was consistent with the elemental compositions of raw U tailing specimens determined by XRF. As shown in Table S6 in the SI, after the leaching experiments, the weight percentages (wt %) of Si in the specimens coming from the Fe(III)−Mn(VII)-participated leaching (EDS e, Figure 5), sequential system (EDS f, Figure 5), and coupling system (EDS g, Figure 5) were 24.20, 32.00, and 34.85%, respectively. Undoubtedly, the EDS results echoed the morphological characterization of the three kinds of specimens (SEM, e−f). The extraction of U in the coupling system was related to the dissolution of Al, Fe, and Mn constituents in the specimen.

3.5. Discussions on the MW-Affected U Leaching Behaviors. U ions were released from the tailing specimen into the dissolution under the influence of pH, oxidants, leaching time, temperatures, and MW in the sequential and coupling systems (Figures 2 and S1, SI). Although more excellent leaching performance for U ions was obtained (Table 1) and verified in the coupling system (Figure 2), the determination of the rate-limiting step for the U extraction was still obscure (Figure 3). The MW irradiation significantly enhanced the Fe(III)−Mn(VII)-participated activation of the mineral dissolution in the tailing specimen in the coupling system (Table S6, SI). Generally, the changes in the mineral compositions and micromorphologies demonstrated that the MW treatment promoted more Fe(III)−Mn(VII) ions to penetrate deeper into the reaction core along with the original pores and cracks distributing on the tailing particles, which facilitated the dissolution of Al, Fe, and Mn constituents in the specimen and left more gangue compositions (i.e., SiO_2) in the particles. The chemical speciation of U in the two treatment systems is shown in Figure 6. Compared with the sequential

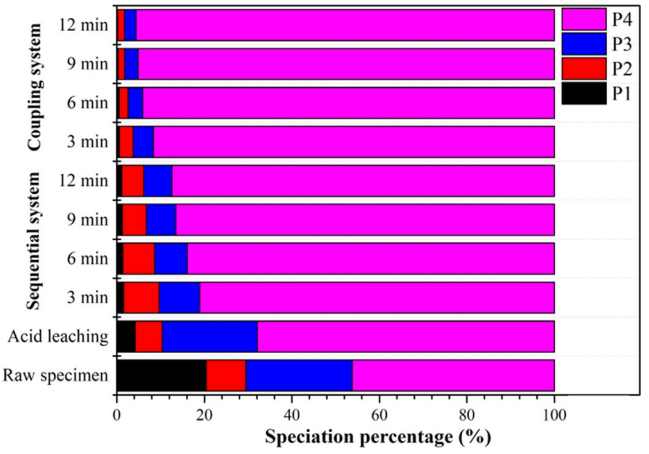

Figure 6. Chemical speciation of U in the sequential and coupling systems (the chemical speciation of U in the tailing specimens was fractionated into four partitions, including acid extractable (P1), reducible (P2), oxidizable (P3), and residual (P4)).

system, higher residual fractions (P4) were obtained in the coupling counterpart with the increases in the MW time. The chemical speciation results supported the mineral and morphological analyses. U ions with more potential mineral constituents were leached from the tailing particles, corresponding to the decreases in the fractions of P1−P3 (Figure 6). The internal migration of oxidant ions into the particle core has strengthened the electron circulation between Fe(III)−Mn(VII) species and the metastable minerals, which further accelerated the dissolution of Al-, Fe-, and Mn-loaded

https://doi.org/10.1021/acsomega.2c02392
ACS Omega 2022, 7, 24574−24586

constituents in the acid conditions (Figure 5). However, the inappropriateness of SCM fittings (Table S5, SI) indicated that some U ions had been reabsorbed to tailing specimens and the particle cores were not shrinking over the whole leaching time in the sequential or coupling system. A contrary increase for the particle core was anticipated in the later stage of experiments (Figure 2).

4. CONCLUSIONS

Although Fe(III) and Mn(VII) showed some degree of adsorption characteristics for U ions, the oxidant-participated leaching experiments in sequential and coupling systems achieved explicitly higher extraction results for U ions compared with those of pure acid processes. Furthermore, the composite oxidants at a ratio of Fe(III) to Mn(VII) of 3 achieved better leaching performance than the single oxidant. In the coupling systems with different oxidants, the significance order of the parametrical variables in the orthogonal design followed as H_2SO_4 concentrations (B, M) > microwave time (A, min) > oxidant concentrations (C, M) > leaching temperatures (E, °C) > leaching time (D, min). The H_2SO_4 concentrations dominatingly affected the leaching processes in the coupling systems with the MW irradiation having a significant influence on the whole process. $A_4B_4C_2D_3E_3$ was quantitively determined by ANOVA as the optimal combination of variables for the coupling system. With the increase of Fe(III) and the participation of Mn(VII), the suitability of the SCM model for the leaching process precipitously declined in the middle and late stages, indicating that the unleached solid cores in the U tailing particles had experienced a reverse increase after the first shrink process over time. Moreover, the characterizations of mineral compositions and morphologies before and after leaching experiments in the two systems supported the internal migration of oxidant ions into the particle cores, which caused the enhancement of U leaching by further accelerating the dissolution of Al, Fe, and Mn constituents in the acid conditions.

■ ASSOCIATED CONTENT

Supporting Information

The Supporting Information is available free of charge at https://pubs.acs.org/doi/10.1021/acsomega.2c02392.

Specifications on the sequential systems; five variables with five levels in the orthogonal design; elemental composition of raw uranium tailing sample (wt %); parametrial results of SCM obtained from fitting analysis; marginal means of variables based on the leaching efficiencies in the orthogonal design; main phases matched in the U tailing specimens; shrinking core model and Arrhenius formula (PDF)

■ AUTHOR INFORMATION

Corresponding Authors

Tao Huang − *School of Safety Engineering, China University of Mining and Technology, Xuzhou 221116, China; School of Materials Engineering, Changshu Institute of Technology, Suzhou 215500, China; Suzhou Key Laboratory of Functional Ceramic Materials, Changshu Institute of Technology, Changshu 215500, China;* orcid.org/0000-0002-8367-1218; Email: ht1104705720@qq.com

Jing Du − *School of Materials Engineering, Changshu Institute of Technology, Suzhou 215500, China*; Email: 286809786@qq.com

Authors

Qingxiang Wang − *School of Safety Engineering, China University of Mining and Technology, Xuzhou 221116, China*

Lulu Zhou − *School of Materials Engineering, Changshu Institute of Technology, Suzhou 215500, China*

Complete contact information is available at: https://pubs.acs.org/10.1021/acsomega.2c02392

Author Contributions

Q.W. and T.H. contributed to the study conception and design. Material preparation, data collection, and analysis were performed by T.H., Q.W., and L.Z. The first draft of the manuscript was written by Q.W. and all authors commented on previous versions of the manuscript. T.H., L.Z., J.D., and Q.W. read and approved the final manuscript.

Funding

This work was funded by the China Postdoctoral Science Foundation (2020M681774) and the Natural Science Foundation of the Jiangsu Higher Education Institutions of China (20KJB490001).

Notes

The authors declare no competing financial interest.

The datasets generated and/or analyzed during the current study are available in the [NAME] repository, [PERSISTENT WEB LINK TO DATASETS]

■ REFERENCES

(1) Liu, S.; Wang, Z.; Lu, Y. X.; Li, H. P.; Chen, X. J.; Wei, G. Y.; Wu, T.; Maguire, D. J.; Ye, G.; Chen, J. Sunlight-induced uranium extraction with triazine-based carbon nitride as both photocatalyst and adsorbent. *Appl Catal., B* **2021**, *282*, No. 119523.

(2) Fiori, F.; Zhou, Z. A study on the Chinese nuclear energy options and the role of ADS reactor in the Chinese nuclear expansion. *Prog. Nucl. Energy* **2016**, *91*, 159−169.

(3) Fiori, F.; Zhou, Z. Sustainability of the Chinese nuclear expansion: Natural uranium resources availability, Pu cycle, fuel utilization efficiency and spent fuel management. *Ann. Nucl. Energy* **2015**, *83*, 246−257.

(4) Li, P.; Chen, P.; Wang, G. H.; Wang, L. Z.; Wang, X. G.; Li, Y. R.; Zhang, W. M.; Jiang, H.; Chen, H. Uranium elimination and recovery from wastewater with ligand chelation-enhanced electrocoagulation. *Chem. Eng. J.* **2020**, *393*, No. 124819.

(5) Jiang, X. Y.; Wang, H. Q.; Hu, E. M.; Lei, Z. W.; Fan, B. L.; Wang, Q. L. Efficient adsorption of uranium from aqueous solutions by microalgae based aerogel. *Microporous Mesoporous Mater.* **2020**, *305*, No. 110383.

(6) Yang, X. J.; Zhang, Z. F.; Kuang, S. T.; Wei, H. Q.; Li, Y. L.; Wu, G. L.; Geng, A. F.; Li, Y. H.; Liao, W. P. Removal of thorium and uranium from leach solutions of ion-adsorption rare earth ores by solvent extraction with Cextrant 230. *Hydrometallurgy.* **2020**, *194*, No. 105343.

(7) Ballini, M.; Chautard, C.; Nos, J.; Phrommavanh, V.; Beaucaire, C.; Besancon, C.; Boizard, A.; Cathelineau, M.; Peiffert, C.; Vercouter, T.; et al. A multi-scalar study of the long-term reactivity of uranium mill tailings from Bellezane site (France). *J. Environ. Radioact.* **2020**, *218*, No. 106223.

(8) Adya, V. C.; Mohapatra, M.; Pathak, N.; Kumar, M.; Hon, N. S.; Thulasidas, S. K.; Kulkarni, M. J.; Natarajan, V. Separation of uranium from solid (U, Pu, Ag) oxide analytical waste: effect of batch size and nitric acid molarity. *J. Radioanal. Nucl. Chem.* **2016**, *308*, 341−345.

(9) Ye, Y. J.; Liu, W.; Li, S.; Huang, C. H.; Guo, Q.; Chung, L. K.; Chen, G. L.; Liu, Y. H. Z. A laboratory method for concurrently determining diffusion migration parameters and water saturation effects of thoron in uranium tailings. *Chemosphere* **2020**, *249*, No. 126520.
(10) Yubo, G.; Zhou, Z. K.; Li, J. M.; Li, G. C.; Chao, L.; Sun, Z. X.; Zheng, L. L.; Yang, Z. H.; Rao, M. M. Combined use of CaCl(2)roasting and nitric acid leaching for the removal of uranium and radioactivity from uranium tailings. *J. Radioanal. Nucl. Chem.* **2020**, *325*, 657−665.
(11) Yin, M. L.; Tsang, D. C. W.; Sun, J.; Wang, J.; Shang, J. Y.; Fang, F.; Wu, Y.; Liu, J.; Song, G.; Xiao, T. F.; Chen, D. Critical insight and indication on particle size effects towards uranium release from uranium mill tailings: Geochemical and mineralogical aspects. *Chemosphere* **2020**, *250*, No. 126315.
(12) Zhang, B.; Li, M.; Zhang, X. W.; Huang, J. Kinetics of Uranium Extraction from Uranium Tailings by Oxidative Leaching. *JOM* **2016**, *68*, 1990−2001.
(13) Tuovinen, H.; Pohjolainen, E.; Vesterbacka, D.; Kaksonen, K.; Virkanen, J.; Solatie, D.; Lehto, J.; Read, D. Release of radionuclides from waste rock and tailings at a former pilot uranium mine in eastern Finland. *Boreal Environ. Res.* **2016**, *21*, 471−480.
(14) Zielenkiewicz, U.; Szczesny, P. Uranium bioleaching - insight into the structure of microbial consortia from mining tailings. *FEBS J.* **2013**, *280*, 570.
(15) Chautard, C.; Beaucaire, C.; Gerard, M.; Roy, R.; Savoye, S.; Descostes, M. Geochemical characterization of uranium mill tailings (Bois Noirs Limouzat, France) highlighting the U and Ra-226 retention. *J. Environ. Radioact.* **2020**, *218*, No. 106251.
(16) Ouyang, J. F.; Liu, Z. R.; Zhang, L.; Wang, Y.; Zhou, L. M. Analysis of influencing factors of heavy metals pollution in farmland-rice system around a uranium tailings dam. *Process Saf. Environ.* **2020**, *139*, 124−132.
(17) Liu, Z. R.; Xiu, T. Y.; Du, Y.; Wang, Y. Leaching characteristics and kinetics of radioactive element uranium and thorium from Ta/Nb tailing. *J. Radioanal. Nucl. Chem.* **2020**, *323*, 1197−1206.
(18) Ma, W. J.; Gao, B.; Guo, Y. D.; Sun, Z. X.; Zhang, Y. H.; Chen, G. X.; Zhu, X. J.; Zhang, C. Y. Occurrence and Distribution of Uranium in a Hydrological Cycle around a Uranium Mill Tailings Pond, Southern China. *Int. J. Environ. Res. Public Health* **2020**, *17*, No. 773.
(19) Ouyang, J. F.; Liu, Z. R.; Ye, T. Z.; Zhang, L. Uranium pollution status and speciation analysis in the farmland-rice system around a uranium tailings mine in southeastern China. *J. Radioanal. Nucl. Chem.* **2019**, *322*, 1011−1022.
(20) Lu, Z.; Liu, Z. R. Pollution characteristics and risk assessment of uranium and heavy metals of agricultural soil around the uranium tailing reservoir in Southern China. *J. Radioanal. Nucl. Chem.* **2018**, *318*, 923−933.
(21) Xun, Y.; Zhang, X. J.; Chaoliang, C.; Luo, X. G.; Zhang, Y. Comprehensive Evaluation of Soil Near Uranium Tailings, Beishan City, China. *Bull. Environ. Contam. Toxicol.* **2018**, *100*, 843−848.
(22) Liu, B.; Peng, T. J.; Sun, H. J. Leaching behavior of U, Mn, Sr, and Pb from different particle-size fractions of uranium mill tailings. *Environ. Sci. Pollut. Res.* **2017**, *24*, 15804−15815.
(23) Dejeant, A.; Bourva, L.; Sia, R.; Galoisy, L.; Calas, G.; Phrommavanh, V.; Descostes, M. Field analyses of U-238 and Ra-226 in two uranium mill tailings piles from Niger using portable HPGe detector. *J. Environ. Radioact.* **2014**, *137*, 105−112.
(24) Essilfie-Dughan, J.; Hendry, M. J.; Warner, J.; Kotzer, T. Arsenic and iron speciation in uranium mine tailings using X-ray absorption spectroscopy. *Appl. Geochem.* **2013**, *28*, 11−18.
(25) Xinwei, H.; Wang, Y. D.; Hu, N.; Sha, Y. H.; Ding, D. X. Bioremediation of effluent from a uranium mill tailings repository in South China by Azolla-Anabaena. *J. Radioanal. Nucl. Chem.* **2018**, *317*, 739−746.
(26) He, L.; Gao, B.; Luo, X.; Jiao, J.; Qin, H. H.; Zhang, C. Y.; Dong, Y. H. Health Risk Assessment of Heavy Metals in Surface Water near a Uranium Tailing Pond in Jiangxi Province, South China. *Sustainability* **2018**, *10*, No. 1113.
(27) Evseeva, T. I.; Maistrenko, T. A.; Belykh, E. S.; Geras'kin, S. A. The assessment of no adverse effect doses for plant populations chronically exposed to radionuclides of uranium and thorium decay series. *Radiatsionnaia Biologiia, Radioecologiia.* **2010**, *50*, 383−390.
(28) Jiang, F. L.; Guo, J. T.; Wang, X. L.; Liu, Y.; Li, X. Y.; Chen, G.; Wang, Z.; Yang, J.; Tan, B. Experimental study on the leaching performance of U(VI) solidified by uranium tailing cement with different admixtures and ratios. *Environ. Technol. Innovation* **2020**, *17*, No. 100506.
(29) Zhou, L.; Dong, F. Q.; Li, H. L.; Huo, T. T.; Wang, P. P.; Liu, M. X.; Yang, G.; Zhang, W.; Hu, W. Y.; Nie, X. Q.; et al. Surface interaction between metazeunerite and an indigenous microorganism Kocuria rosea: Implications for bioremediation of As-U tailings. *Chem. Eng. J.* **2019**, *359*, 393−401.
(30) Jiang, F. L.; Chen, G.; Li, M.; Liu, Y.; Li, X. Y.; Guo, J. T.; Wu, H. N.; Wang, Z. Experimental study of different admixture effects on the properties of uranium mill tailing solidified bodies. *J. Radioanal. Nucl. Chem.* **2019**, *322*, 1159−1168.
(31) Robertson, J.; Hendry, M. J.; Kotzer, T.; Hughes, K. A. Geochemistry of uranium mill tailings in the Athabasca Basin, Saskatchewan, Canada: A review. *Crit. Rev. Environ. Sci. Technol.* **2019**, *49*, 1237−1293.
(32) Laxman Singh, K.; Sudhakar, G.; Swaminathan, S. K.; Rao, C. M. Identification of elite native plants species for phytoaccumulation and remediation of major contaminants in uranium tailing ponds and its affected area. *Environ. Dev. Sustainable* **2015**, *17*, 57−81.
(33) Huang, T.; Su, Z.; Dai, Y.; Zhou, L. Enhancement of the heterogeneous adsorption and incorporation of uraniumVI caused by the intercalation of β-cyclodextrin into the green rust. *Environ. Pollut.* **2021**, *290*, No. 118002.
(34) Jiang, F. L.; Wang, Z.; Chen, G.; Liu, Y.; Wu, H. N.; Tan, B. A.; Luo, C. W. Experimental study of pore characteristics and radon exhalation of uranium tailing solidified bodies in acidic environments. *Environ. Sci. Pollut. Res.* **2021**, *28*, No. 20111.
(35) Kaksonen, A. H.; Boxall, N. J.; Gumulya, Y.; Khaleque, H. N.; Morris, C.; Bohu, T.; Cheng, K. Y.; Usher, K. M.; Lakaniemi, A. M. Recent progress in biohydrometallurgy and microbial characterisation. *Hydrometallurgy.* **2018**, *180*, 7−25.
(36) Werner, A.; Meschke, K.; Bohlke, K.; Daus, B.; Haseneder, R.; Repke, J. U. Resource Recovery from Low-Grade Ore Deposits and Mining Residuals by Biohydrometallurgy and Membrane Technology Potentials and Case Studies. *ChemBioEng Rev.* **2018**, *5*, 6−17.
(37) Saleh, H. M.; Aglan, R. F.; Mahmoud, H. H. Qualification of corroborated real phytoremediated radioactive wastes under leaching and other weathering parameters. *Prog. Nucl. Energy* **2020**, *119*, No. 103178.
(38) Bayoumi, T. A.; Saleh, H. M. Characterization of biological waste stabilized by cement during immersion in aqueous media to develop disposal strategies for phytomediated radioactive waste. *Prog. Nucl. Energy* **2018**, *107*, 83−89.
(39) Yan, X.; Luo, X. G. Uptake of uranium, thorium, radium and potassium by four kinds of dominant plants grown in uranium mill tailing soils from the southern part of China. *Radioprotection* **2016**, *51*, 141−144.
(40) Favas, P. J. C.; Pratas, J.; Varun, M.; D'Souza, R.; Paul, M. S. Accumulation of uranium by aquatic plants in field conditions: Prospects for phytoremediation. *Sci Total Environ.* **2014**, *470−471*, 993−1002.
(41) Huang, T.; Song, D. P.; Yin, L. X.; Zhang, S. W.; Liu, L. F.; Zhou, L. L. Microwave irradiation assisted sodium hexametaphosphate modification on the alkali-activated blast furnace slag for enhancing immobilization of strontium. *Chemosphere* **2020**, *241*, No. 125069.
(42) Huang, T.; Zhou, L. L.; Chen, L.; Liu, W. H.; Zhang, S. W.; Liu, L. F. Mechanism exploration on the aluminum supplementation coupling the electrokinetics-activating geopolymerization that re-

https://doi.org/10.1021/acsomega.2c02392
ACS Omega 2022, 7, 24574−24586

inforces the solidification of the municipal solid waste incineration fly ashes. *Waste Manage.* **2020**, *103*, 361−369.
(43) Wang, B. M.; Fan, C. C. Hydration behavior and immobilization mechanism of MgO-SiO2-H2O cementitious system blended with MSWI fly ash. *Chemosphere.* **2020**, *250*, No. 126269.
(44) Mohammad Eisa, H.; Vaezi, I.; Ardakani, A. M. Evaluation of solidification/stabilization in arsenic-contaminated soils using lime dust and cement kiln dust. *Bull. Eng. Geol. Environ.* **2020**, *79*, 1683−1692.
(45) Yakubu, Y.; Zhou, J.; Shu, Z.; Zhang, Y.; Wang, W. B.; Mbululo, Y. Potential application of pre-treated municipal solid waste incineration fly ash as cement supplement. *Environ. Sci. Pollut. Res.* **2018**, *25*, 16167−16176.
(46) Huang, C. M.; Li, M.; Zhang, X. W.; Gao, F. Y.; Wu, X. Y.; Fang, Q.; Tan, W. F.; Zhang, D. Uranium Extraction from Tailings by Dilute Alkali Pretreatment-Sulfuric Acid Leaching Technology. *JOM* **2018**, *70*, 2746−2752.
(47) Brindha, K.; Elango, L.; Rajesh, R. Characterisation of Uranium Mining and Tailings Pond Areas by Integrated Remote Sensing, Geophysical, Geological and Hydrogeological Methods. *J. Geol. Soc. India* **2020**, *95*, 377−384.
(48) Li, M.; Gao, F. Y.; Zhang, X. W.; Lv, S. Y.; Huang, J.; Wu, X. Y.; Fang, Q. Recovery of uranium from low-grade tailings by electro-assisted leaching. *J. Cleaner Prod.* **2020**, *271*, No. 122639.
(49) Li, Z. Z.; Hadioui, M.; Wilkinson, K. J. Conditions affecting the release of thorium and uranium from the tailings of a niobium mine. *Environ Pollut.* **2019**, *247*, 206−215.
(50) Liu, B.; Peng, T. J.; Sun, H. J.; Yue, H. J. Release behavior of uranium in uranium mill tailings under environmental conditions. *J. Environ. Radioact.* **2017**, *171*, 160−168.
(51) Ahmad, A. A.; Al-Raggad, M.; Shareef, N. Production of activated carbon derived from agricultural by-products via microwave-induced chemical activation: a review. *Carbon Lett.* **2021**, *31*, 957−971.
(52) Zhou, C. B.; Zhang, Y. W.; Liu, Y.; Deng, Z. Y.; Li, X. T.; Wang, L.; Dai, J. J.; Song, Y. M.; Jiang, Z. H.; Qu, J. S.; Siyal, A. A. Co-pyrolysis of textile dyeing sludge and red wood waste in a continuously operated auger reactor under microwave irradiation. *Energy* **2021**, *218*, No. 119398.
(53) Flesoura, G.; Dilissen, N.; Dimitrakis, G.; Vleugels, J.; Pontikes, Y. A new approach for the vitrification of municipal solid waste incinerator bottom ash by microwave irradiation. *J. Cleaner Prod.* **2021**, *284*, No. 124787.
(54) Sun, Y. F.; Hu, S. G.; Zhang, P.; Elmaadawy, K.; Ke, Y.; Li, J. H.; Li, M. Y.; Hu, J. P.; Liu, B. C.; Yang, J. K.; et al. Microwave enhanced solidification/stabilization of lead slag with fly ash based geopolymer. *J. Cleaner Prod.* **2020**, *272*, No. 122957.
(55) Kumari, M.; Jain, Y.; Yadav, P.; Laddha, H.; Gupta, R. Synthesis of Fe3O4-DOPA-Cu Magnetically Separable Nanocatalyst: A Versatile and Robust Catalyst for an Array of Sustainable Multi-component Reactions under Microwave Irradiation. *Catal. Lett.* **2019**, *149*, 2180−2194.
(56) Park, S.; Byoun, Y.; Kang, H.; Song, Y. J.; Choi, S. W. ZnO Nanocluster-Functionalized Single-Walled Carbon Nanotubes Synthesized by Microwave Irradiation for Highly Sensitive NO2 Detection at Room Temperature. *ACS Omega* **2019**, *4*, 10677−10686.
(57) Hu, G. Z.; Sun, C.; Huang, J. X.; Xu, G.; Zhu, J. Q. Evolution of Shale Microstructure under Microwave Irradiation Stimulation. *Energy Fuels* **2018**, *32*, 11467−11476.
(58) Usman, M.; Byrne, J. M.; Chaudhary, A.; Orsetti, S.; Hanna, K.; Ruby, C.; Kappler, A.; Haderlein, S. B. Magnetite and Green Rust: Synthesis, Properties, and Environmental Applications of Mixed-Valent Iron Minerals. *Chem. Rev.* **2018**, *118*, 3251−3304.
(59) Bhave, C.; Shejwalkar, S. A review on the synthesis and applications of green rust for environmental pollutant remediation. *Int. J. Environ. Sci. Technol.* **2018**, *15*, 1243−1248.
(60) Ghosh, A.; Foster, J. M.; Offer, G.; Marinescu, M. A Shrinking-Core Model for the Degradation of High-Nickel Cathodes (NMC811) in Li-Ion Batteries: Passivation Layer Growth and Oxygen Evolution. *J Electrochem. Soc.* **2021**, *168*, No. 020509.
(61) Gao, F. Y.; Li, M.; Zhang, X. W.; Huang, C. M.; Wu, X. Y.; Zhou, Y. C.; Fang, Q. Liberation Mechanism of Uranium from Radioactive Metallurgical Waste Containing Uranium by a Clean Leaching Method. *JOM* **2020**, *72*, 3491−3501.
(62) Zou, Z.; Yan, D.; Zhu, J. Y.; Zheng, Y. P.; Li, H. Z.; Zhu, Q. S. Simulation of the Fluid-Solid Noncatalytic Reaction Based on the Structure-Based Mass-Transfer Model: Shrinking Core Reaction. *Ind. Eng. Chem. Res.* **2020**, *59*, 17729−17739.
(63) Hidalgo, T.; Kuhar, L.; Beinlich, A.; Putnis, A. Kinetics and mineralogical analysis of copper dissolution from a bornite/chalcopyrite composite sample in ferric-chloride and methanesulfonic-acid solutions. *Hydrometallurgy* **2019**, *188*, 140−156.
(64) Valeev, D.; Kunilova, I.; Shoppert, A.; Salazar-Concha, C.; Kondratiev, A. High-pressure HCl leaching of coal ash to extract Al into a chloride solution with further use as a coagulant for water treatment. *J. Cleaner Prod.* **2020**, *276*, 123206.
(65) Nikic, J.; Watson, M.; Tubic, A.; Isakovski, M. K.; Maletic, S.; Mohora, E.; Agbaba, J. Arsenic removal from water using a one-pot synthesized low-cost mesoporous Fe-Mn-modified biosorbent. *J. Serb. Chem. Soc.* **2019**, *84*, 327−342.
(66) Szlachta, M.; Chubar, N. The application of Fe-Mn hydrous oxides based adsorbent for removing selenium species from water. *Chem. Eng. J.* **2013**, *217*, 159−168.
(67) Xiao, F. Z.; Wang, C.; Yu, L. M.; Pu, Y. Q.; Xu, Y. L.; Zhang, K.; Luo, J. Q.; Zhu, Q. Q.; Chen, F.; Liu, Y.; et al. Fabrication of magnetic functionalised calix[4]arene composite for highly efficient and selective adsorption towards uranium(VI). *Environ Chem.* **2019**, *16*, 577−586.
(68) Ding, L.; Tan, W. F.; Xie, S. B.; Mumford, K.; Lv, J. W.; Wang, H. Q.; Fang, Q.; Zhang, X. W.; Wu, X. Y.; Li, M. Uranium adsorption and subsequent re-oxidation under aerobic conditions by Leifsonia sp - Coated biochar as green trapping agent. *Environ. Pollut.* **2018**, *242*, 778−787.
(69) Singh, J.; Singh, S. P. Geopolymerization of solid waste of non-ferrous metallurgy - A review. *J Environ Manage.* **2019**, *251*, No. 109571.
(70) Firdous, R.; Stephan, D.; Djobo, J. N. Y. Natural pozzolan based geopolymers: A review on mechanical, microstructural and durability characteristics. *Constr. Build. Mater.* **2018**, *190*, 1251−1263.
(71) Rao, F.; Liu, Q. Geopolymerization and Its Potential Application in Mine Tailings Consolidation: A Review. *Miner. Process. Extr. Metall. Rev.* **2015**, *36*, 399−409.
(72) Zhuang, X. Y.; Chen, L.; Komarneni, S.; Zhou, C. H.; Tong, D. S.; Yang, H. M.; Yu, W. H.; Wang, H. Fly ash-based geopolymer: clean production, properties and applications. *J. Cleaner Prod.* **2016**, *125*, 253−267.
(73) Huang, T.; Zhang, S. W.; Liu, L. F.; Zhou, L. L. Green rust functionalized geopolymer of composite cementitious materials and its application on treating chromate in a holistic system. *Chemosphere* **2021**, *263*, No. 128319.
(74) El-Habaak, G.; Askalany, M.; Abdel-Hakeem, M. The effect of mineralogy of calcined shales on the alkali activation and geopolymerization reactions: A case study from Abu-Tartur plateau, Western Desert, Egypt. *Appl. Clay Sci.* **2018**, *162*, 90−100.
(75) Eyvazi, B.; Jamshidi-Zanjani, A.; Darban, A. K. Immobilization of hexavalent chromium in contaminated soil using nano-magnetic MnFe2O4. *J. Hazard. Mater.* **2019**, *365*, 813−819.
(76) Tang, S. F.; Li, X.; Zhang, C.; Liu, Y.; Zhang, W. T.; Yuan, D. Strengthening decomposition of oxytetracycline in DBD plasma coupling with Fe-Mn oxide-loaded granular activated carbon. *Plasma Sci. Technol.* **2019**, *21*, No. 025504.

https://doi.org/10.1021/acsomega.2c02392
ACS Omega 2022, 7, 24574−24586